Extraction of the Lateral Position of Border Traps in Nanoscale MOSFETs

Yury Illarionov, *Graduate Student Member, IEEE*, Markus Bina, Stanislav Tyaginov, Karina Rott, Ben Kaczer, Hans Reisinger, and Tibor Grasser, *Senior Member, IEEE*

***Abstract*— A novel method for the extraction of the lateral position of border traps in nanoscale MOSFETs is presented. Using technology computer-aided design (TCAD) simulations, we demonstrate that the dependence of the trap-induced threshold voltage shift on the drain bias is more sensitive to the lateral trap position than to the impact of random dopants. Based on this, the lateral defect position can be determined with a precision of several percent of the channel length. To demonstrate the correct functionality of our technique, we apply it to extract the lateral positions of experimentally observed traps. Although the most accurate algorithm is based on time-consuming TCAD simulations, we propose a simplified analytic expression, which allows for the extraction of the lateral trap position directly from the experimental data. While the uncertainty introduced by random dopants is <10% for the TCAD model, the additional errors introduced by the simple analytic expression still provide trap positions accurate to 5% for the devices with 20-nm channel length and 20%–25% for 100-nm-long devices.**

***Index Terms*— Charged traps, defect position, nanoscale MOSFETs, random dopants, threshold voltage shift.**

I. Introduction

CHARGED traps near the oxide/silicon interface and in the oxide bulk can have a dramatic impact on the characteristics of modern MOSFETs [1]–[11]. Although nanoscale transistors contain very few defects [8], each of them can significantly disturb the channel electrostatics and affect the device performance. In particular, the lifetime of a device [2], [11] is ultimately determined by a time-dependent variability of the transistor characteristics that are caused by the creation/annealing and/or the charging/discharging of interface and oxide traps. Consequently, one must study the device reliability from a statistical point of view. Therefore, much information about the energy levels of border traps [10]–[12] and their depth distribution in the oxide film [5] has been presented recently. However, there is no study related to the extraction of the lateral defect position that considers the impact of random dopants. This information is significant because charged traps situated in different regions of the device may have a significantly different impact on the device performance depending on the applied bias conditions. In particular, our experiments performed on pMOSFETs show that the magnitude of the threshold voltage shift induced by the border traps and its dependence on the drain bias can be dramatically different and strong (Fig. 1). It is this drain voltage dependence of the threshold voltage shift which we will exploit in the following to extract the lateral position of the traps.

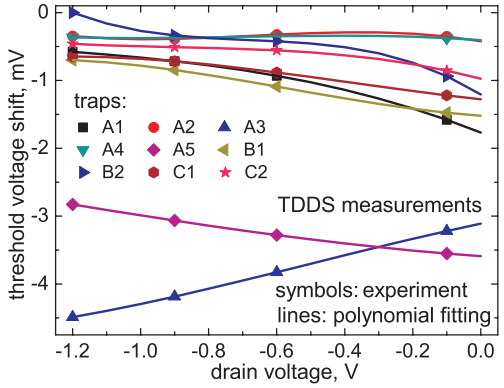

Fig. 1. $\Delta V_{\rm th}(V_d)$ characteristics of nine individual traps obtained from TDDS measurements [13]–[15] on pMOSFET with a channel length of $L = 100$ nm and 2.2-nm thick SiON film employed as a gate insulator. The results can be perfectly fitted using the cubic polynomial function $\Delta V_{\rm th}(V_d) = \sum_i p_i V_d^i$.

Several attempts to evaluate the trap position have been undertaken so far [4], [5], [16]–[20]. One of the most recent trap location techniques is the 2-D trap profiling method based on the drain-induced barrier lowering (DIBL) effect, which is described in [16]. This technique employs a relation between the position of the channel barrier peak and the magnitude of random telegraph noise (RTN). However, it does not account for the significant impact of the border traps and the random dopants on the shape of the potential profile. In Fig. 2, we demonstrate that this effect may significantly affect the shape of the channel barrier, which would make the relation for the peak position evaluated in [16] inapplicable, independently of the magnitude of the DIBL effect. Another technique based on RTN analysis has been proposed in [5]. However, it focuses on the evaluation of the defect depth in the oxide rather than

Manuscript received February 6, 2015; revised June 29, 2015; accepted July 4, 2015. Date of current version August 19, 2015. This work was supported in part by the Austrian Science Fund through the FWF under Project p23958 and in part by the European Commission FP7 under Project 261868. The review of this paper was arranged by Editor E. Rosenbaum.

Y. Illarionov and S. Tyaginov are with the Institute for Microelectronics, Vienna University of Technology, Vienna 1040, Austria, and also with the Ioffe Physical-Technical Institute, Saint Petersburg 194021, Russia (e-mail: illarionov@iue.tuwien.ac.at; tyaginov@iue.tuwien.ac.at).

M. Bina and T. Grasser are with the Institute for Microelectronics, Vienna University of Technology, Vienna 1040, Austria (e-mail: bina@iue.tuwien.ac.at; grasser@iue.tuwien.ac.at).

K. Rott and H. Reisinger are with Infineon Technologies, Neubiberg 85579, Germany (e-mail: karina.rott@infineon.com; hans.reisinger@infineon.com).

B. Kaczer is with imec, Leuven 3001, Belgium (e-mail: kaczer@imec.be).

Color versions of one or more of the figures in this paper are available online at http://ieeexplore.ieee.org.

Digital Object Identifier 10.1109/TED.2015.2454433

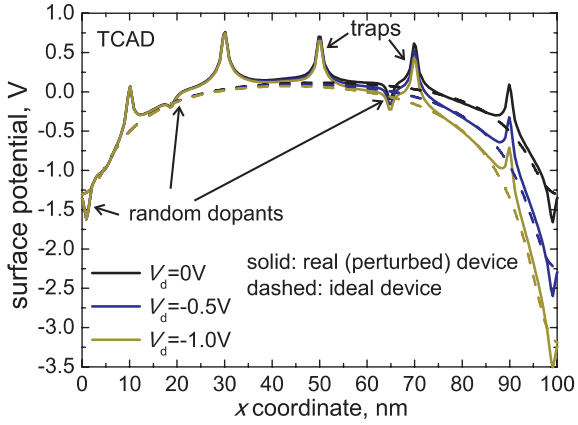

Fig. 2. Surface potential distribution along the interface of the investigated device with five traps situated exactly at the interface and randomly distributed dopants overlaid on the similar distribution for an ideal device, i.e., without traps and random dopants. The TCAD simulations have been performed in the weak inversion regime ($V_g = -0.2$ V). The source corresponds to $x = 0$ nm and the drain to $x = 100$ nm.

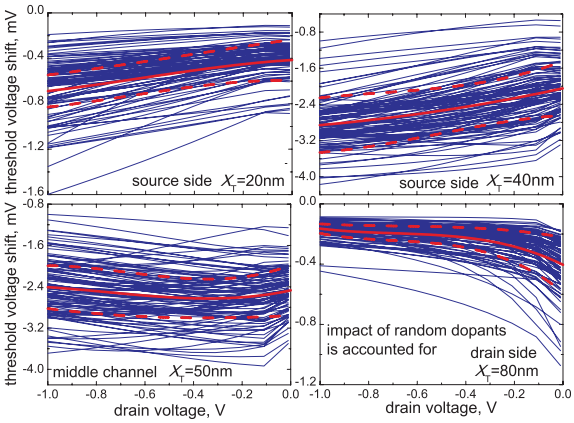

Fig. 3. $\Delta V_{\rm th}(V_d)$ characteristics for devices with one hundred different random dopant configurations and four different lateral trap coordinates X_T simulated using TCAD. Red lines: characteristics with average (solid) and plus/minus standard deviation cubic parameterization coefficients (dashed). Clearly, the shape of the $\Delta V_{\rm th}(V_d)$ curves is more strongly affected by the lateral trap position than by the random dopant distribution, which impacts mostly the absolute value. Therefore, it can be used as a defect fingerprint and allows to evaluate the lateral defect coordinate.

the lateral position. At the same time, the information on the lateral trap position would allow to understand the role of each single trap in its contribution to the device performance.

In this paper, we introduce a new approach, which exploits the fact that the impact of the lateral defect coordinate X_T on the drain bias dependence of the threshold voltage shift $\Delta V_{\rm th}$ induced by a single charged trap is stronger than the impact of random dopants. Accounting for the effect of random dopants is the key feature of our approach since it allows us to estimate the evaluation uncertainty for each of the extracted lateral trap positions. The accuracy of our method is discussed using the experimental data provided in Fig. 1. In addition, we introduce a simple equation, which allows to estimate the lateral trap position with a reasonable accuracy directly from the experimental data given in Fig. 1.

II. Experiment

The pMOSFETs with $W/L = 150/100$ nm and 2.2-nm-thick SiON films have been characterized using time-dependent defect spectroscopy (TDDS) [13]–[15]. This technique is based on alternatively charging and discharging preexisting border traps in order to study their capture and emission times. While having the same properties as newly created defects [21], in pMOSFETs, these traps are responsible for the recoverable component of the negative bias-temperature instability. By analyzing the TDDS results, the threshold voltage shift $\Delta V_{\rm th}$ versus the applied drain bias V_d, induced by each particular trap, can be individually traced. Results for three different devices and nine defects are summarized in Fig. 1. One can see that the $\Delta V_{\rm th}(V_d)$ characteristics of every single trap have dramatically different shapes. Since the trap depth and energy level has no significant impact on the drain bias dependence of $\Delta V_{\rm th}$ [22], this indicates that the traps responsible for the threshold voltage shift are located in different regions of the device [4]. Based on this assumption, we perform a parameterization of the $\Delta V_{\rm th}(V_d)$ curves and demonstrate that they can be perfectly approximated by a cubic polynomial function of V_d. As will be shown later, the corresponding parameterization coefficients are unique for each particular trap position. Therefore, this unique set of coefficients can be treated as the defect signature and used for a precise evaluation of the lateral defect coordinate.

III. TCAD Simulations

We apply our technology computer-aided design (TCAD) simulator Minimos-NT that considers random discrete dopants using the established methodology pioneered in [23] with a density gradient model [24] to account for the quantum correction of the Coulomb potential [25]. This simulator has already been successfully applied to assess the reliability of modern nanoscale devices [26], [27]. The TCAD simulations were performed for one hundred devices with identical architectures but with different configurations of random dopants. The lateral defect coordinate along the oxide/silicon interface (X_T) was varied from the source to the drain using 10-nm steps to provide the benchmark for our trap location technique. At the same time, it was found that the trap coordinate in the direction perpendicular to the source-bulk-drain plane has no significant impact on the shape of the $\Delta V_{\rm th}(V_d)$ curves. Therefore, in all our simulations, we used $W_T = W/2$. This implies, however, that W_T can not be extracted using our methodology. At the same time, a weak dependence of the results on the position across the channel W_T, together with an insignificant impact of the vertical trap position on the $\Delta V_{\rm th}(V_d)$ dependence [22], means that the impact of shallow trench isolation [28] on our results is negligible as well. The $\Delta V_{\rm th}$ values induced by the traps situated in each particular position were evaluated as a function of V_d for all 100 devices using I_d–V_g curves simulated with and without charged traps. Evaluation of $\Delta V_{\rm th}$ has been performed using a standard method [29] for a fixed I_d corresponding to $V_g \leq V_{\rm th}$, i.e., weak inversion.

The obtained $\Delta V_{\rm th}(V_d)$ curves show a cubic behavior, just like their experimental counterparts. In Fig. 3, one can clearly

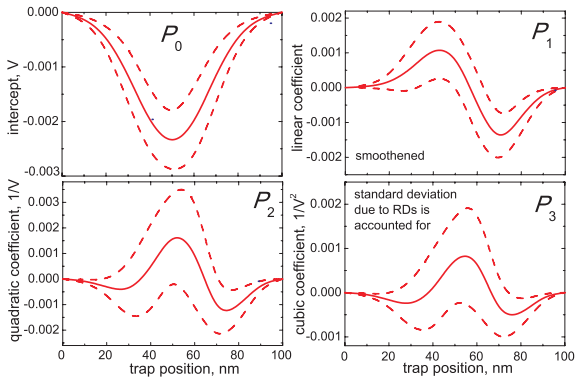

Fig. 4. Dependences of the polynomial parameterization coefficients of the $\Delta V_{\rm th}(V_d)$ characteristics on X_T simulated with TCAD (interpolation using 0.1-nm steps and smoothing is done). Clearly, the behavior of the $\Delta V_{\rm th}(V_d)$ curves is different for different lateral defect coordinates. The impact of random dopants is accounted for; the solid lines reflect the average values and the dashed ones the average plus/minus σ_i.

see that the shape of these curves has a stronger dependence on the lateral defect coordinate X_T than on the distribution of random dopants. For example, if a trap is situated at the source side of the channel ($X_T = 20$ nm and $X_T = 40$ nm), $\Delta V_{\rm th}$ versus V_d increases independently of the configuration of random dopants. However, for a trap situated at the drain side ($X_T = 80$ nm) $\Delta V_{\rm th}$ versus V_d decreases. When a trap is located in the middle of the channel ($X_T = 50$ nm), the situation becomes more complicated. Although for most of the random dopant configurations the dependence of $\Delta V_{\rm th}$ on V_d is mostly dominated by the higher order polynomial terms, for some of them $\Delta V_{\rm th}$ increases versus V_d while for others it decreases. This is because the transition between the two possible types of $\Delta V_{\rm th}(V_d)$ dependence takes place for trap positions close to the middle of the channel, although the exact point is determined by the random dopant configuration. In [30], the observed behavior of the $\Delta V_{\rm th}(V_d)$ curves for different X_T values has been captured using a compact model, which treats a charged defect as a local increase of the channel doping concentration.

The correlation between the $\Delta V_{\rm th}(V_d)$ characteristics and the lateral trap position is the working principle of our trap location technique. Clearly, the expected accuracy of our technique for the central traps is lower, since the dependence of the $\Delta V_{\rm th}(V_d)$ behavior on the random dopant configuration is strongest.

IV. Method Description

In order to extract the lateral trap position from the experimental data, we parameterize the results of the TCAD simulations using a cubic polynomial function $\Delta V_{\rm th}(V_d) = \sum_i P_i V_d^i$. The coefficients P_i are determined for each random dopant configuration corresponding to a certain X_T. The mean TCAD coefficients $\langle P_i \rangle$ and $\langle P_i \rangle \pm \sigma_i$, with σ_i being the standard deviations induced by the random dopants, are subsequently calculated. Their dependences on the lateral defect position are shown in Fig. 4. Note that although in the simulations X_T has been varied using 10-nm steps, the values of P_i have been then interpolated at all intermediate X_T points using 0.1-nm steps. The lateral trap position is evaluated according to an algorithm that compares the cubic parameterization coefficients p_i, obtained from the experimental data (Fig. 1), to those P_i which are simulated using TCAD.

The principle of our trap location technique is shown in Fig. 5. For each X_T, one can find a minimum k_i which guarantees that p_i lies inside the interval $[\langle P_i \rangle - k_i\sigma_i; \langle P_i \rangle + k_i\sigma_i]$. Therefore, the proximity between experimental and TCAD data will be reflected by the sum $K = \sum_i k_i$. The parameter K is a function of the lateral defect coordinate X_T that reaches its minimum value when the combination of p_i lies closest to the corresponding $\langle P_i \rangle$ [Fig. 5 (left)]. Since it is supposed that the $\Delta V_{\rm th}(V_d)$ curve obtained from TDDS measurements is associated with an individual defect, the corresponding value of X_T is considered as the most likely extracted lateral position of this defect.

After the lateral defect position is evaluated, the probability that all four intervals $[\langle P_i \rangle - k_i\sigma_i; \langle P_i \rangle + k_i\sigma_i]$ obtained for the extracted X_T do not simultaneously overlap with their counterparts for neighboring points, $X_{T\rm left}$ and $X_{T\rm right}$, is determined. This probability is interpreted as the probability that the trap is situated inside the interval $[X_{T\rm left}, X_{T\rm right}]$ centered at the extracted X_T [Fig. 5 (center)]. Then, the obtained probability can be replotted in terms of a normalized density [Fig. 5 (right)], which is obtained for each X_T and dX as a probability to find the trap inside the fixed interval $[X_T - dX; X_T + dX]$. Note that the consideration of all four coefficients results in high accuracy of the lateral trap position evaluation. This is because the proximity of the experimental coefficients to their TCAD counterparts is determined more reliably, while the neighboring points can be separated with a higher probability, which increases the resolution.

As follows from the above description, the accuracy of our trap location technique depends on the impact of random dopants on the shape of $\Delta V_{\rm th}(V_d)$. Since the impact of random dopants is known to be stronger in devices with smaller L [23], one could expect that the method will not allow for an accurate extraction of X_T in ultrascaled devices. However, the results of our TCAD simulations (Fig. 6) show that the magnitude and drain bias dependence of $\Delta V_{\rm th}$ are considerably more sensitive to X_T if a device with smaller L is considered. Moreover, the increase in the magnitude of the X_T-dependence is stronger compared with the increase in the magnitude of the random dopant fluctuations, which will lead to an even higher precision for ultrascaled devices. Therefore, below we operate with a relative accuracy, which is given in percentage of L.

V. Method Verification

In order to verify the correct functionality of the described trap location technique, we check if the reverse algorithm reproduces the benchmark X_T. For this purpose, we select one of the $\Delta V_{\rm th}(V_d)$ curves simulated by TCAD for a certain configuration of random dopants. Initially, we examine the curve that is closest to the mean for the considered benchmark X_T. This characteristic is used as experimental data for our algorithm. In this way, the optimum accuracy of the method can be evaluated. The procedure has been repeated for numerous lateral defect coordinates along the channel.

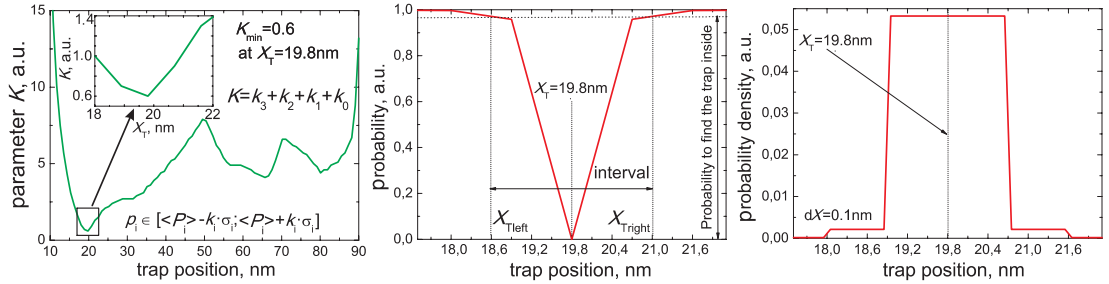

Fig. 5. Illustration of the working principle of our trap location algorithm for $X_T = 20$ nm. Left: typical $K(X_T)$ dependence. K determines the proximity of the experimental $\Delta V_{\rm th}(V_d)$ to the mean curve simulated using TCAD or the compact model. $K_{\rm min}$ is observed at $X_T = 19.8$ nm, which is the most likely lateral defect position. Center: probability to find the trap inside several intervals around an extracted X_T. This is equivalent to the probability with which the points $X_{T\rm left}$, X_T, and $X_{T\rm right}$ can be separated with respect to the narrowest intervals $[\langle P_i\rangle - k_i\sigma_i;\ \langle P_i\rangle + k_i\sigma_i]$ selected at each point. Right: probability density corresponding to the interval $dX = 0.1$ nm. The origin of this distribution is due to the uncertainity introduced by the random dopants.

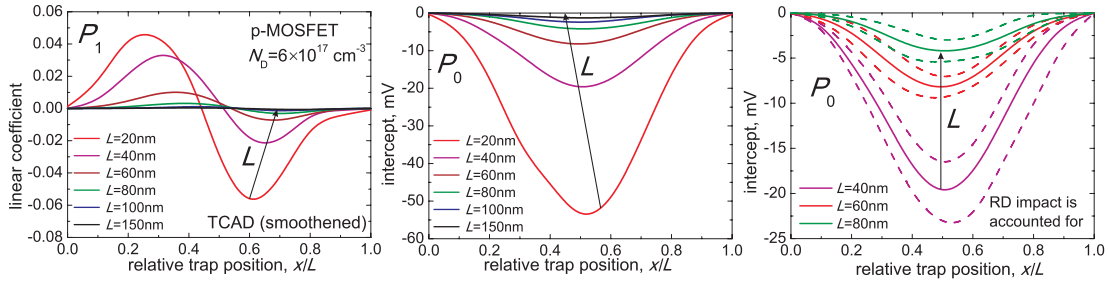

Fig. 6. Dependences of the slope and the intercept of the $\Delta V_{\rm th}(V_d)$ characteristics on X_T simulated with TCAD for devices with different channel lengths. Clearly, for smaller L, the impact of the lateral trap position on the magnitude and drain bias dependence of $\Delta V_{\rm th}$ increases more significantly than the magnitude of random dopant fluctuations (right plot). Therefore, although in ultrascaled devices the impact of random dopants is more pronounced [23], device scaling will even lead to an improvement in the accuracy of our trap location technique.

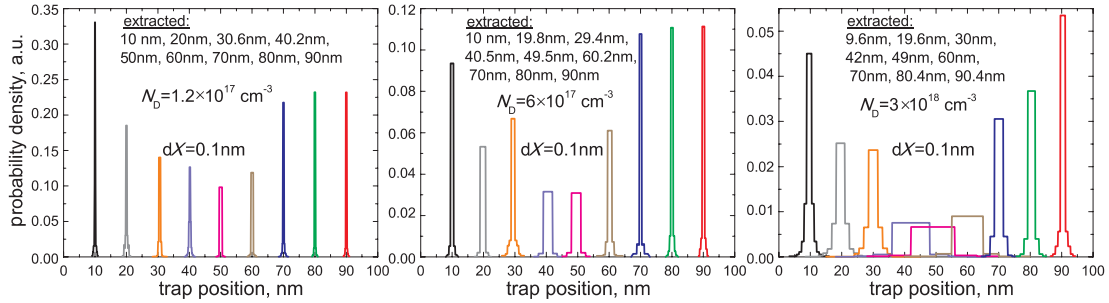

Fig. 7. Probability densities obtained for similar devices with three different channel doping levels. The algorithm is applied to the $\Delta V_{\rm th}(V_d)$ characteristic, which is closest to the mean TCAD curve. Therefore, the results reflect the best accuracy that can be achieved with our trap location technique for different sections of the device channel (benchmark X_T is varied between 10 and 90 nm using 10-nm steps). In all cases, the impact of random dopants is stronger in the middle of the channel. The best overall accuracy is reached for the device with the lowest N_D.

In addition, devices with different channel doping levels N_D have been examined. The obtained results, plotted in terms of the probability densities, are given in Fig. 7. One can see that in all cases the error in the extracted X_T rarely exceeds 2% of L. However, for the traps located near the middle of the channel, the distributions are broader and their heights are lower. This is because the fluctuations of $\Delta V_{\rm th}$ induced by random dopants are more significant [31]. The observed behavior of the probability density can be well described by a Gaussian distribution. The reason for a small deviation is that the precision of the algorithm is limited by several percents of L, especially in the middle of the channel. Another important feature is that the accuracy of our technique decreases with increasing channel doping. This originates from a weaker $\Delta V_{\rm th}(V_d)$ dependence observed for devices with high N_D. Therefore, the impact of random dopants is more pronounced, which leads to a broadening of the probability distributions.

As a further verification step, we repeat the procedure with characteristics that strongly deviate from the mean. In such a case, the $\Delta V_{\rm th}(V_d)$ curves are considerably displaced from the mean curve, i.e., the deviation of the parameterization coefficients from $\langle P_i\rangle$ is stronger. The obtained probability density distributions are plotted in Fig. 8. They correspond to border traps situated at $X_T = 20$ nm (top) and at $X_T = 20$ nm (bottom). The $\Delta V_{\rm th}(V_d)$ characteristics with $P_i = \langle P_i\rangle \pm \sigma_i$ and $\langle P_i\rangle \pm 3\sigma_i$ were examined. One can see that the uncertainty in the extracted lateral trap position for coefficients spread within $[\langle P_i\rangle - \sigma_i,\ \langle P_i\rangle + \sigma_i]$, which are the most common for the considered devices, does not exceed 5%. For the case of an extremely strong impact of random dopants, when the $\Delta V_{\rm th}(V_d)$ shape strongly deviates from the mean (i.e., $[\langle P_i\rangle - 3\sigma_i,\ \langle P_i\rangle + 3\sigma_i]$), the error rarely exceeds 10%, even if the trap is situated in the middle of the channel. This is still better than our knowledge about technological

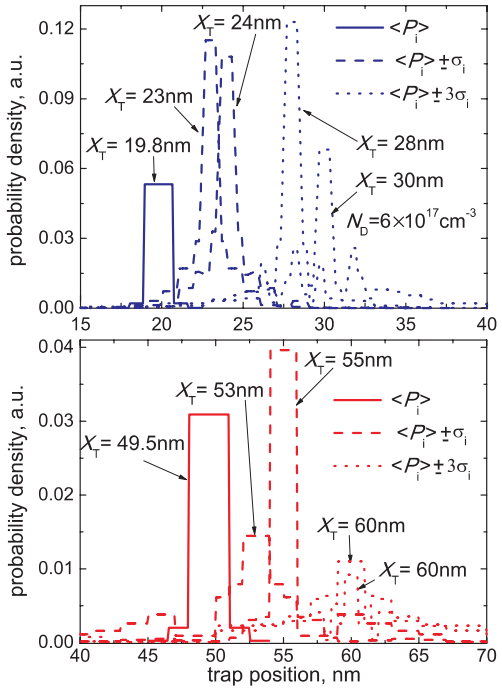

Fig. 8. Dependence of the accuracy of our trap location technique on the deviation of $\Delta V_{\rm th}(V_d)$ curve from the mean, i.e., the severity of random dopant configuration. The plotted probability densities ($dX = 0.1$ nm) correspond to border traps situated at $X_T = 20$ nm (top) and $X_T = 20$ nm (bottom). The lateral defect coordinate extracted for the ideal case ($P_i = \langle P_i \rangle$) is nearly the same as the benchmark X_T. For a stronger impact of random dopants ($P_i = \langle P_i \rangle \pm \sigma_i$) the uncertainty is ∼3%–5%, and for extremely severe random dopant configurations ($P_i = \langle P_i \rangle \pm 3\sigma_i$) it is ∼8%–10%.

parameters of the transistors such as doping profiles and thus sufficient for the practical application of our method to characterize industrial MOSFETs.

VI. Simplified Algorithm

The use of TCAD allows for the simulation of the reference data for the trap location technique with a rather high accuracy. However, the technique requires substantial computational resources. Therefore, in [30], we attempted to reproduce the observed behavior of the $\Delta V_{\rm th}(V_d)$ curves for different X_T using a compact model which exploits the fact that the impact of a charged trap is equivalent to a local increase of the channel doping concentration by several orders of magnitude (see [4], [32]–[34]). Using the perturbed shape of the surface potential we calculated the concentration profiles and implemented them into the Enz–Krummenacher–Vittoz model [35], in order to simulate the I_d–V_g curves and extract $\Delta V_{\rm th}(V_d)$ dependences. Here, we suggest an even more efficient way to simplify our trap location algorithm without a significant loss in accuracy.

This further simplification of our technique is based on the realization that the main information regarding the lateral trap coordinate is given by the slope P_1 and the intercept P_0. The sign of the former determines whether the trap is at the source or at the drain side of the channel and the magnitude of the latter is responsible for the proximity of the trap to one of the electrodes. Knowing that the mean dependence of P_0 on the lateral trap position X_T has a universal shape, which is

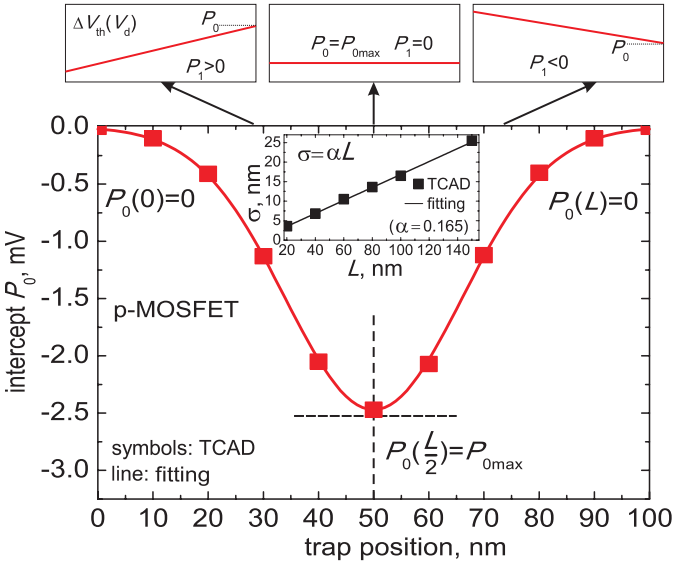

Fig. 9. Knowing that the intercept $P_0 = \Delta V_{\rm th}(V_d = 0)$ is zero near the electrodes and a maximum in the middle of the channel, one can approximate the mean TCAD simulated dependence $P_0(X_T)$ with a Gaussian and derive a simple relation for the relative lateral trap position (2). Inset: standard deviation σ (1) is empirically found to be proportional to L with a coefficient α. The input data that are necessary to estimate X_T are the value of $P_{0\rm max}$, which is extracted for the $\Delta V_{\rm th}(V_d)$ curve belonging to a trap situated in the middle of the channel (top center plot), and the values of P_0 for all other curves together with the corresponding slope signs (top right and left plots). Although the mean $P_0(X_T)$ curve can be fitted almost exactly, for devices that deviate from the mean some uncertainty will be introduced by random dopants.

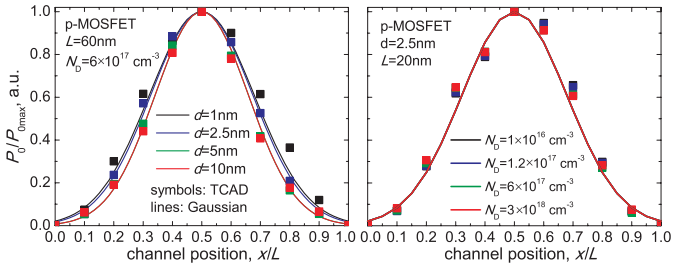

Fig. 10. Gaussian fitting of the mean TCAD simulated dependences $P_0(X_T)$ normalized to $P_{0\rm max}$ for different gate oxide thicknesses (left) and doping concentrations (right) allows to conclude that the parameter α is almost independent of d and N_D, which mainly impact the magnitude of experimentally measured $P_{0\rm max}$.

symmetric with respect to the middle of the channel (e.g., our simulations (Fig. 4) or [4], [31]), we can approximate it using a Gaussian function (Fig. 9)

$$P_0(X_T) = P_{0\rm max} \exp\left(-\frac{\left(X_T - \frac{L}{2}\right)^2}{2\sigma^2}\right) \tag{1}$$

where it is assumed that $P_{0\rm max} = P_0(X_T = L/2)$ and $P_0(X_T = 0) = P_0(X_T = L) = 0$. Based on TCAD simulations performed for devices with different L, the standard deviation σ is found to be proportional to the channel length L as $\sigma = \alpha L$ with $\alpha \approx 0.17$ [Fig. 9 (inset)]. Therefore, the relative lateral trap position can be estimated by

$$\frac{X_T}{L} = \frac{1}{2} - \text{sign}(P_1)\sqrt{2\alpha^2 \log\left(\frac{P_{0\rm max}}{P_0}\right)}. \tag{2}$$

Interestingly, the gate oxide thickness d and channel doping N_D mainly impact the values of $P_{0\rm max}$ that have to be

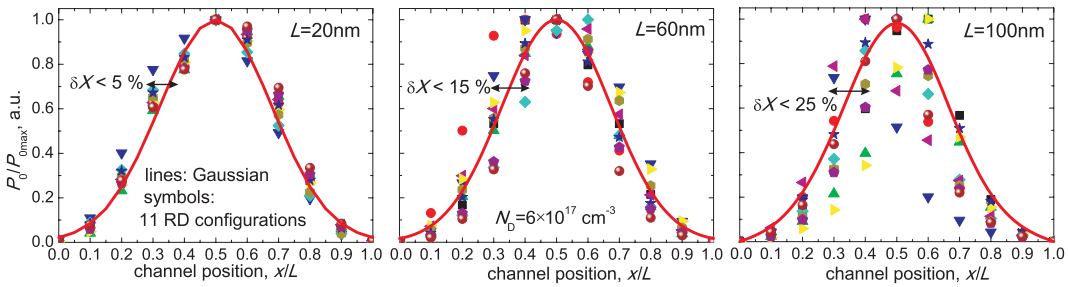

Fig. 11. Gaussian fitting of the mean TCAD simulated dependences $P_0(X_T)$ normalized to $P_{0\max}$ and overlaid on the related dependences obtained with TCAD for certain random dopant configurations. Clearly, with smaller L, the uncertainty is significantly smaller. This makes our simplified technique even better suited for the characterization of border traps in ultrascaled devices.

measured experimentally. At the same time, the parameter α is almost independent of these quantities (Fig. 10).

However, an exact Gaussian fitting of the $P_0(X_T)$ dependence is possible only for the case $P_0 = \langle P_0 \rangle \pm n\sigma_0$ with σ_0 being a standard deviation and n constant along the channel. In reality, for each channel coordinate the values of P_0 can be randomly distributed within the interval $[\langle P_0 \rangle - 3\sigma_0; \langle P_0 \rangle + 3\sigma_0]$, due to the impact of random dopants. Therefore, for a certain random dopant configuration the shape of $P_0(X_T)$ dependences may deviate from a Gaussian, which introduces some uncertainty. In Fig. 11, it is illustrated that this uncertainty δX decreases from below 25% for $L = 100$ nm toward below 5% for $L = 20$ nm. This is because the increase in the magnitude and coordinate dependence of P_0 for devices with smaller L is more significant than an increase in the magnitude of random dopant fluctuations (see Fig. 6). Therefore, our simplified technique is even more suitable for ultrascaled devices.

As a remark one should note that the exact point at which P_1 changes its sign is also affected by the random dopants and can deviate within 5% from the middle of the channel (see Fig. 4). This may lead to a wrong determination of the channel side at which the trap is situated, but only for central traps. Therefore, some additional uncertainty of ~10% has to be noted for these traps.

The input data, necessary to estimate the lateral trap position X_T using (2) can easily be extracted from the experimental results. The value of $P_{0\max}$ is determined only once for each device from the $\Delta V_{\rm th}(V_d)$ characteristic corresponding to the middle of the channel ($X_T = L/2$). This curve typically has a near-zero slope P_1 and the largest among all other values for the intercept P_0; therefore it can easily be discerned. Knowing the value of $P_{0\max}$, one can analyze all other $\Delta V_{\rm th}(V_d)$ curves from the considered data set in order to extract P_0 and sign(P_1) [Fig. 9 (top)] and then apply (2) to estimate X_T.

The necessary condition for the successful application of the simplified modification of our trap location technique is to have at least one $\Delta V_{\rm th}(V_d)$ curve corresponding to $X_T = L/2$ within the experimental data set (i.e., with $P_0 = P_{0\max}$ and $P_1 = 0$). However, considering that modern nanoscale MOSFETs may contain only a limited number of defects [8], one can imagine a situation when such a curve is not available. In particular, this is the case of our experimental data set provided in Fig. 1. In such a case, one can perform a visual analysis of all the measured curves $\Delta V_{\rm th}(V_d)$, in order to find the one, which corresponds to the trap situated closest to the middle of the channel. Such a curve will have the largest P_0 and at the same time the smallest P_1. In the case of Fig. 1 this will be trap A5. Then, this $\Delta V_{\rm th}(V_d)$ curve must be used to determine the value of $P_{0\max}$, which will allow to extract the positions of all other traps using (2).

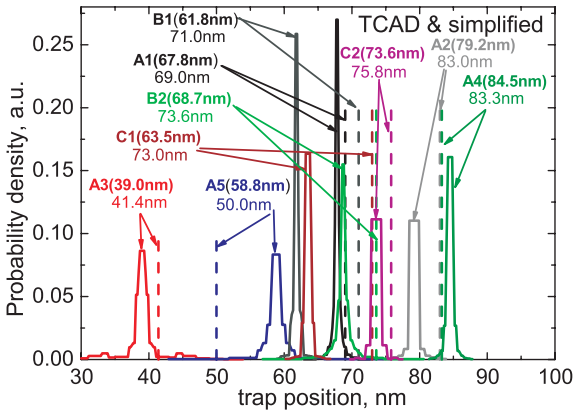

Fig. 12. Probability densities of the lateral trap position calculated for small intervals $dX = 0.2$ nm for the experimental data given in Fig. 1. The results obtained using TCAD data (solid lines) are compared with the estimations done using the simplified method (dashed lines). The difference in the extracted values of X_T is always <10% of the channel length (100 nm).

Alternatively, one can perform a visual qualitative analysis of the experimental traces (Fig. 1) and immediately recognize that the $\Delta V_{\rm th}(V_d)$ curves where $P_1 > 0$ and $P_1 < 0$ correspond to traps situated at the source side and the drain side of the channel, respectively. Moreover, traps with a larger P_0 are situated closer to the middle of the channel while those with a smaller P_0 are closer to the electrodes.

VII. Results and Discussion

We have applied our trap location technique to the experimental results given in Fig. 1 (pMOSFET, $L \approx 100$ nm, $N_D \approx 6 \times 10^{17}$ cm^{-3}) and extracted the positions of all nine individual traps, which have been detected. First, we employed the results of our TCAD simulations as a reference. The obtained probability density distributions are plotted in Fig. 12. The results demonstrate that the traps can be located with a rather high accuracy inside narrow intervals. The width

of these intervals is typically related to the impact of the random dopants. For this reason, the obtained distributions are broader for traps close to the middle of the channel where the device is more sensitive to random dopants. In the same plot, the values of X_T estimated using our simplified trap location method (2) are given. The value of $P_{0\max}$ has been estimated from the $\Delta V_{\rm th}(V_d)$ curve corresponding to the trap A5, which is the closest to $X_T = L/2$. Although the simplified technique does not allow for any probability calculations and leads to a single value of X_T, the results are very similar to those obtained using TCAD data. The typical difference in the extracted X_T values in all cases is $<10\%$, while an accuracy is even expected to be improved for smaller devices. Therefore, considering that the TCAD simulations require several weeks of cluster simulations and that the simplified algorithm gives the results in several minutes, we conclude that the substitution of the precise algorithm with the simplified one is quite appropriate if one needs to increase the efficiency.

We finally remark that although all the above is based on the results obtained for pMOSFETs, it is obvious that our trap location technique can be used for nMOSFETs as well. The main thing one should note is that in the case of nMOSFET $\Delta V_{\rm th}$ is positive.

VIII. Conclusion

We have suggested a precise method for the extraction of the lateral position of traps in nanoscale MOSFETs, which accounts for the impact of random dopants. Our approach exploits the fact that the slope and curvature of the trap-induced threshold voltage shift versus drain bias of a single trap is considerably less sensitive to the random dopants as opposed to the lateral trap position. Based on this we have demonstrated that the lateral defect coordinate can be estimated with a precision of several percents of the channel length. In addition, we introduced a simple expression, which allows for the estimation of the lateral trap position directly from the experimental data and demonstrated that the extraction uncertainty decreases for devices with smaller channel length. Therefore, the simplified version of our technique can avoid time-consuming TCAD simulations and considerably increase the efficiency of the entire procedure. Finally, we have demonstrated the applicability of our trap location technique using experimental data.

Acknowledgment

The authors would like to thank L. Filipovic for valuable discussions.

References

[1] A. J. Lelis and T. R. Oldham, "Time dependence of switching oxide traps," *IEEE Trans. Nucl. Sci.*, vol. 41, no. 6, pp. 1835–1843, Dec. 1994.

[2] R. Dreesen *et al.*, "A new degradation model and lifetime extrapolation technique for lightly doped drain nMOSFETs under hot-carrier degradation," *Microelectron. Rel.*, vol. 41, no. 3, pp. 437–443, 2001.

[3] P. M. Lenahan, "Atomic scale defects involved in MOS reliability problems," *Microelectron. Eng.*, vol. 69, nos. 2–4, pp. 173–181, 2003.

[4] A. Asenov, R. Balasubramaniam, A. R. Brown, and J. H. Davies, "RTS amplitudes in decananometer MOSFETs: 3-D simulation study," *IEEE Trans. Electron Devices*, vol. 50, no. 3, pp. 839–845, Mar. 2003.

[5] S. Lee, H.-J. Cho, Y. Son, D. S. Lee, and H. Shin, "Characterization of oxide traps leading to RTN in high-k and metal gate MOSFETs," in *Proc. IEEE Int. Electron Devices Meeting (IEDM)*, Dec. 2009, pp. 1–4.

[6] T. Grasser *et al.*, "Switching oxide traps as the missing link between negative bias temperature instability and random telegraph noise," in *Proc. IEEE Int. Electron Devices Meeting (IEDM)*, Dec. 2009, pp. 1–4.

[7] A. T. M. G. Sarwar, M. R. Siddiqui, R. H. Siddique, and Q. D. M. Khosru, "Effects of interface traps and oxide traps on gate capacitance of MOS devices with ultrathin (EOT $\sim$ 1 nm) high-κ stacked gate dielectrics," in *Proc. IEEE TENCON*, Jan. 2009, pp. 1–5.

[8] B. Kaczer, P. J. Roussel, T. Grasser, and G. Groeseneken, "Statistics of multiple trapped charges in the gate oxide of deeply scaled MOSFET devices—Application to NBTI," *IEEE Electron Device Lett.*, vol. 31, no. 5, pp. 411–413, May 2010.

[9] T. Grasser *et al.*, "The paradigm shift in understanding the bias temperature instability: From reaction–diffusion to switching oxide traps," *IEEE Trans. Electron Device*, vol. 58, no. 11, pp. 3652–3666, Nov. 2011.

[10] M. Toledano-Luque, B. Kaczer, P. Roussel, M. J. Cho, T. Grasser, and G. Groeseneken, "Temperature dependence of the emission and capture times of SiON individual traps after positive bias temperature stress," *J. Vac. Sci. Technol. B*, vol. 29, no. 1, pp. 01AA04-1–01AA04-5, 2011.

[11] M. Toledano-Luque, B. Kaczer, T. Grasser, P. J. Roussel, J. Franco, and G. Groeseneken, "Toward a streamlined projection of small device bias temperature instability lifetime distributions," *J. Vac. Sci. Technol. B*, vol. 31, no. 1, pp. 01A114-1–01A114-4, 2013.

[12] D. M. Fleetwood, "'Border traps' in MOS devices," *IEEE Trans. Nucl. Sci.*, vol. 39, no. 2, pp. 269–271, Apr. 1992.

[13] T. Grasser *et al.*, "Advanced characterization of oxide traps: The dynamic time-dependent defect spectroscopy," in *Proc. IEEE Int. Rel. Phys. Symp. (IRPS)*, Apr. 2013, pp. 2D.2.1–2D.2.7.

[14] T. Grasser, H. Reisinger, P.-J. Wagner, and B. Kaczer, "Time-dependent defect spectroscopy for characterization of border traps in metal-oxide-semiconductor transistors," *Phys. Rev. B*, vol. 82, pp. 245318-1–245318–10, Dec. 2010.

[15] M. Waltl, P.-J. Wagner, H. Reisinger, K. Rott, and T. Grasser, "Advanced data analysis algorithms for the time-dependent defect spectroscopy of NBTI," in *Proc. IEEE Int. Integr. Rel. Workshop (IIRW)*, Oct. 2012, pp. 74–79.

[16] E. R. Hsieh, Y. L. Tsai, S. S. Chung, C. H. Tsai, R. M. Huang, and C. T. Tsai, "The understanding of multi-level RTN in trigate MOSFETs through the 2D profiling of traps and its impact on SRAM performance: A new failure mechanism found," in *IEDM Tech. Dig.*, 2012, pp. 19.2.1–19.2.4.

[17] H.-J. Cho, S. Lee, B.-G. Park, and H. Shin, "Extraction of trap energy and location from random telegraph noise in gate leakage current (I_g RTN) of metal–oxide semiconductor field effect transistor (MOSFET)," *Solid-State Electron.*, vol. 54, no. 4, pp. 362–367, 2010.

[18] S. Park *et al.*, "Extracting accurate position and energy level of oxide trap generating random telegraph noise (RTN) in recessed channel MOSFET's," in *Proc. ESSDERC*, 2010, pp. 337–340.

[19] D. Kang, J. Kim, D. Lee, B.-G. Park, J. D. Lee, and H. Shin, "Extraction of vertical, lateral locations and energies of hot-electrons-induced traps through the random telegraph noise," *Jpn. J. Appl. Phys.*, vol. 48, no. 4S, pp. 04C034-1–04C034-4, 2009.

[20] H.-J. Kang, M.-K. Jeong, S.-M. Joe, B.-G. Park, and J.-H. Lee, "Characterization of random telegraph noise generated in the space region in NAND flash memory strings," *Semicond. Sci. Technol.*, vol. 29, no. 12, pp. 125001-1–125001-6, 2014.

[21] T. Grasser *et al.*, "On the volatility of oxide defects: Activation, deactivation, and transformation," in *Proc. IEEE Int. Rel. Phys. Symp. (IRPS)*, Apr. 2015, pp. 5A.3.1–5A.3.8.

[22] T. Grasser, "Stochastic charge trapping in oxides: From random telegraph noise to bias temperature instabilities," *Microelectron. Rel.*, vol. 52, no. 1, pp. 39–70, 2012.

[23] A. Asenov, "Random dopant induced threshold voltage lowering and fluctuations in sub-0.1 μm MOSFET's: A 3-D 'atomistic' simulation study," *IEEE Trans. Electron Devices*, vol. 45, no. 12, pp. 2505–2513, Dec. 1998.

[24] M. G. Ancona, N. S. Saks, and D. McCarthy, "Lateral distribution of hot-carrier-induced interface traps in MOSFETs," *IEEE Trans. Electron Devices*, vol. 35, no. 12, pp. 2221–2228, Dec. 1988.

[25] A. R. Brown *et al.*, "Use of density gradient quantum corrections in the simulation of statistical variability in MOSFETs," *J. Comput. Electron.*, vol. 9, no. 3, pp. 187–196, 2010.

[26] M. Bina, O. Triebl, B. Schwarz, M. Karner, B. Kaczer, and T. Grasser, "Simulation of reliability on nanoscale devices," in *Proc. SISPAD*, 2012, pp. 109–112.
[27] M. Bina *et al.*, "Predictive hot-carrier modeling of n-channel MOSFETs," *IEEE Trans. Electron Devices*, vol. 61, no. 9, pp. 3103–3110, Sep. 2014.
[28] Y.-H. Lee, T. Linton, K. Wu, and N. Mielke, "Effect of trench edge on pMOSFET reliability," *Microelectron. Rel.*, vol. 41, no. 5, pp. 689–696, 2001.
[29] B. Kaczer, V. Arkhipov, R. Degraeve, N. Collaert, G. Groeseneken, and M. Goodwin, "Disorder-controlled-kinetics model for negative bias temperature instability and its experimental verification," in *Proc. 43rd Annu. IEEE Int. Rel. Phys. Symp. (IRPS)*, Apr. 2005, pp. 381–387.
[30] Y. Y. Illarionov *et al.*, "A reliable method for the extraction of the lateral position of defects in ultra-scaled MOSFETs," in *Proc. IEEE Int. Rel. Phys. Symp. (IRPS)*, Jun. 2014, pp. XT.13.1–XT.13.6.
[31] T. Cochet, T. Skotnicki, G. Ghibaudo, and A. Poncet, "Lateral dependence of dopant-number threshold voltage fluctuations in MOSFETs," in *Proc. 29th ESSDERC*, 1999, pp. 680–683.
[32] A. Ghetti, M. Bonanomi, C. M. Compagnoni, A. S. Spinelli, A. L. Lacaita, and A. Visconti, "Physical modeling of single-trap RTS statistical distribution in flash memories," in *Proc. IEEE Int. Rel. Phys. Symp. (IRPS)*, Apr./May 2008, pp. 610–615.
[33] A. Ghetti *et al.*, "Scaling trends for random telegraph noise in deca-nanometer flash memories," in *Proc. IEEE Int. Electron Device Meeting (IEDM)*, Dec. 2008, pp. 1–4.
[34] A. Ghetti, C. M. Compagnoni, A. S. Spinelli, and A. Visconti, "Comprehensive analysis of random telegraph noise instability and its scaling in deca–nanometer flash memories," *IEEE Trans. Electron Devices*, vol. 56, no. 8, pp. 1746–1752, Aug. 2009.
[35] G. V. Angelov and K. K. Asparuhova, "MOSFET simulation using MATLAB implementation of the EKV model," in *Proc. ELECTRONICS*, 2006, pp. 167–172.

Yury Illarionov was born in Saint Petersburg, Russia, in 1988. He received the M.Sc. degrees from Saint Petersburg State Polytechnical University, Saint Petersburg, in 2011, and the FAME Erasmus Mundus Program, in 2012, and the Ph.D. degree from the Ioffe Physical-Technical Institute, Saint Petersburg, in 2015. In 2013, he joined the Institute for Microelectronics (TU Wien, Austria).

His current research interests include tunnel MIS structures, and Si and 2-D FETs reliability issues.

Markus Bina received the Ph.D. degree in electrical and biomedical engineering from the Technische Universität Wien, Austria, in 2014. During his doctoral studies, he worked on charge carrier transport, BTI, channel hot-carrier effects and variability in semiconductor devices, publishing several papers on these topics. Since late 2014 he is working for Infineon Technologies on semiconductor power devices.

His scientific interests include charge carrier transport, power devices, and reliability of semiconductor devices.

Stanislav Tyaginov was born in Saint Petersburg, Russia, in 1978. He received the M.Sc. degree in 2002, and the Ph.D. degree, in 2006.

He joined the Institute for Microelectronics, Vienna University of Technology, Vienna, Austria, in 2008. He has been a Post-Doctoral Researcher with the Ioffe Physical-Technical Institute, Saint Petersburg. His current research interests include the device modeling, modeling of HCD and TDDB, and tunneling phenomena in MOS devices.

Karina Rott received the Diploma degree in technical physics from the Gdansk University of Technology, Gdańsk, Poland, in 2006. She is currently pursuing the Ph.D. degree in electrical engineering with the Vienna University of Technology, Vienna, Austria.

Ms. Rott has been with the Device Reliability Department, Infineon, Neubiberg, Germany, since 2011, involved in N-/PBTI phenomena. She is currently with the Infineon's Dielectric Reliability Department and is involved in IGBT degradation.

Ben Kaczer is a Principal Scientist at imec, Belgium. He received the Ph.D. degree in physics from The Ohio State University, in 1998. He has co-authored over 350 journal and conference papers and two patents, and received seven IEEE IRPS and IPFA Best and Outstanding Paper Awards and the 2011 IEEE EDS Paul Rappaport Award. He is currently serving on the IEEE Transactions on Electron Devices Editorial Board.

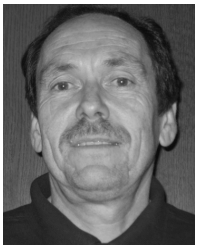

Hans Reisinger received the Diploma degree in physics and the Ph.D. degree from the Technical University of Munich, Munich, Germany, in 1979 and 1983, respectively.

He has been with Infineon, Neubiberg, Germany, since 1986, where he is involved in thin dielectrics and interfaces in DRAMs and NVMs. He is currently with the Infineon's reliability Department and is involved in MOSFET degradation.

Tibor Grasser an Associate Professor at TU Wien, is the co-author or author of more than 500 scientific articles, editor of books on advanced device simulation, the bias temperature instability (Springer), and hot carrier degradation (Springer) and received the Best and Outstanding Paper Awards at IRPS, IPFA, and ESREF, and the IEEE EDS Paul Rappaport Award.